Biophysical Journal Volume 93 October 2007 2781–2790

Structural Features that Govern Enzymatic Activity in Carbonic Anhydrase from a Low-Temperature Adapted Fish, *Chionodraco hamatus*

Stefano Marino,* Kuniko Hayakawa,*† Keisuke Hatada,† Maurizio Benfatto,† Antonia Rizzello,‡ Michele Maffia,‡ and Luigi Bubacco*

*Department of Biology, University of Padova, Padua, Italy; †Laboratori Nazionali di Frascati dell'Istituto Nazionale de Fisica Nucleare, INFN, c.p. 13, Frascati, Italy; and ‡Department of Biological and Environmental Science and Technology, University of Salento, Lecce, Italy

ABSTRACT The carbonic anhydrase (CA) family of zinc metalloenzymes includes many known isozymes that have different subcellular distributions. The study described here focuses on identification of the structural features that define low-temperature adaptation in a *Chionodraco hamatus* protein, both for the reaction center, at an atomic level, and for the tertiary structure of the protein. To this aim, an x-ray absorption near-edge spectroscopy/Minuit x-ray absorption near-edge spectroscopy analysis of the reaction center was undertaken for both a structurally characterized human CAII and CA of *C. hamatus*. Higher structural levels were analyzed by sequence comparison and homology modeling. To establish whether the structural insights acquired in fish CAs are general, theoretical models were generated by homology modeling for three temperate-climate-adapted fish CAs. The measured structural differences between the two proteins are discussed in terms of the differences in the electrostatic potential between human CAII and CA of *C. hamatus*. We conclude that modulation of the interaction between the catalytic water molecule and the zinc ion could depend on the effect of the electrostatic potential distribution.

INTRODUCTION

The carbonic anhydrase (CA) family of zinc metalloenzymes includes many known isozymes divided into five distinct classes (α, β, γ, δ, and ε) that appear to have evolved independently (1–3). In mammals, only the α class isoforms are found with different subcellular distributions: cytoplasmic (CAI, CAII, CAIII, CAVII, and CAXIII), plasma-membrane-associated (CAIV, CAIX, CAXII, CAXIV, and CAXV), mitochondrial (CA, VA, and VB), or secreted (CAVI) (1,4,5). CAs catalyze the hydration of carbon dioxide to yield a bicarbonate ion and a proton. This reaction occurs through several chemical steps (6–8). The first is a nucleophilic attack of the zinc-bound hydroxide ion on the substrate CO_2, followed by the exchange of the product bicarbonate ion with a water molecule. The metal-bound hydroxide ion is regenerated by transfer of a proton to bulk solvent. The rate constant k_{cat} generally reflects proton transfer between zinc-bound water and an active-site ''shuttle'' residue, and the subtle structural differences among the CA isozymes contribute to define a wide range of k_{cat} values (10^3–10^6 s^{-1}) measured for this rate-limiting step. Different residues may function as the intermediary proton shuttle between zinc-bound water and bulk solvent in isozymes.

There are several crystal structures of CAs in the PDB (Protein Data Bank) and for vertebrate enzymes, most of them mammalian CAII (with or without a bound inhibitor). Crystallographic structures are also available for both mammalian CAI (again, with or without a bound inhibitor) and CAIII (the S-glutathiolated form of rat CAIII). All of these structures provide key insights into structure-function relationships for this enzyme (9). The zinc cofactor is placed at the base of the conical active-site cleft, where it is coordinated to three histidine residues and one water molecule to yield a tetrahedral geometry. At physiological pH, the fourth zinc ligand is a hydroxide molecule that acts as a nucleophile to catalyze the hydrolysis of CO_2 and esters (at a rate near to the limit imposed by substrate diffusion) (10).

Other important structural features relate to residues that either protrude into the catalytic cleft or contribute to generate a hydrophobic pocket in which the substrate seems to be held. Among the former, the proton shuttle mentioned above plays a key role in the catalytic process. For instance, His^{64} is the catalytic proton shuttle in CAII ($k_{cat} = 10^6$ s^{-1}) (11,12) and the tautomerization of this residue can mediate the transfers of both protons and water molecules at a neutral pH with high efficiency, requiring no time- or energy-consuming processes (13). The side chain of His^{200} is the best candidate for a proton shuttle in CAI ($k_{cat} = 2 \times 10^5$ s^{-1}) (14) due to its proximity to the zinc ion and to the observed pKa value (15). In contrast, it seems that no proton shuttle is present in the active site of CAIII ($k_{cat} = 1 \times 10^4$ s^{-1}), in which the product proton is probably transferred directly to the bulk solvent (16).

The active-site cleft is split into hydrophobic and hydrophilic regions. Mutagenesis and structural analyses of the hydrophobic pocket adjacent to the zinc-bound hydroxide indicate that this region is the site of CO_2 association and that hydrophobicity modulates the catalytic activity (10,17). The proposed association would place the substrate at ~3 Å from the zinc atom. There is a well-defined hydrophobic pocket adjacent to the zinc-bound hydroxide group. The amino acids involved are Trp^{209}, Val^{121}, and Leu/Phe^{198}, which define the

Submitted February 23, 2007, and accepted for publication June 5, 2007.

Address reprint requests to Luigi Bubacco, Dept. of Biology, University of Padova, Viale Ugo Bassi 58B, 35121, Padua, Italy. Tel.: 0039-049-8276346; Fax: 0039-049-8276300; E-mail: luigi.bubacco@unipd.it.

Editor: Jill Trewhella.

0006-3495/07/10/2781/10 $2.00

doi: 10.1529/biophysj.107.107540

mouth and the side, plus Val^{143}, which defines the bottom. The amino acids that define the hydrophobic pocket are completely conserved in carbonic anhydrase II (with Leu^{198}) and CAIII (with Phe^{198}). It has been proposed that steric effects occurring at the mouth of the pocket justify the lower catalytic activity measured for CAIII; these seem to depend on Phe^{198} (18).

Among the polar residues of the active site, the hydroxyl group of the Thr-l99 side chain forms hydrogen bonds with the zinc-hydroxide group and the Glu^{106} side chain to form a Zn-OH-/Thr^{199}/Glu^{106} hydrogen bond network (17,19), which is completely conserved in all animal carbonic anhydrase isozymes. It has been postulated that the hydrogen bond between Thr^{199} and zinc-hydroxide is important to maintain the orientation and reactivity of the zinc-hydroxide group (20), catalyzing proton transfer and discriminating between protic and aprotic anions (21).

Amino acid substitutions at position 65 of CAII demonstrate that the size of the side chain is critical in the assembly of a bridging solvent network between the zinc-bound solvent and the shuttle residue, His^{64}. In particular, the presence in position 65 of either alanine (as in human CAII) or serine (as in almost all other vertebrate CAII) is compatible with a high proton-shuttling rate for the adjacent His^{64} (12,22).

Considering more physiological aspects, carbonic anhydrase plays a crucial role in the excretion of metabolic CO_2 in all vertebrates. In fish, CO_2 produced in the tissues is rapidly hydrated to HCO_3^- by the action of erythrocyte CA. The generated HCO_3^- then diffuses into the blood stream, where it accounts for almost 98% of the total carbon dioxide stored and transported in the plasma (23,24). At the respiratory epithelia in gills or skin, CA catalyzes the rapid dehydration of HCO_3^- to molecular CO_2, which then diffuses passively into the ventilatory water stream. The CO_2/HCO_3^- system constitutes the most important physiological buffers for acid-base regulation (25).

The Antarctic icefish of the family Channichthyidae (suborder Notothenioidei), to which *Chionodraco hamatus* belongs, are a unique example of adult vertebrates lacking hemoglobin and functionally active erythrocytes, and possessing only a small number of erythrocytelike cells (26).The absence of hemoglobin does not represent a dramatic limitation to oxygen transport in the icefish. On the other hand, the very limited number of erythrocytelike cells (and circulating CA) may compromise the CO_2/HCO_3^- equilibrium in the blood (27). However, the elevated solubility of CO_2 in water at low temperatures, and the unusual characteristics of the circulatory system of icefish, contributes to an efficient excretion of CO_2. In teleosts, CA has been found in various tissues. It appears to be present in high concentrations in the gills (28), where it plays an important role in osmoregulation, nitrogen (ammonia) excretion, acid-base balance, and gas exchange (29). Comparisons between the activity of *C. hamatus* gill CA (Ice-CA), another icefish *Trematomus bernacchii* (an Antarctic fish with hemoglobin and red blood cells), and the temperate-adapted fish *Anguilla anguilla* showed that CA activity for the fish lacking hemoglobin is high at temperatures up to 30°C. Above this temperature, activity decreases dramatically, becoming virtually absent at 37°C. At this temperature, *A. anguilla* CA is still at its maximum level of activity (30). With these data, we were particularly interested in identification of the structural features that define low-temperature adaptation in the *C. hamatus* protein, for both the reaction center and the tertiary structure of the protein, at an atomic level. An x-ray absorption near-edge spectroscopy (XANES)/MXAN analysis of the reaction center was undertaken for both a structurally characterized human CAII (hCAII) and for Ice-CA (SWISS-PROT accession number P83299). The higher structural levels were analyzed by sequence comparison and homology modeling. To evaluate the general applicability of the structural insights acquired by our study of CAs, we created some theoretical models using homology modeling, generated for three temperate-climate-adapted fish CAs.

EXPERIMENTAL PROCEDURES

Protein purification

Cytoplasmic Ice-CA from *C. hamatus* gill filaments was obtained as previously described (30). Ice-CA was purified by fast protein liquid chromatography (FPLC) affinity chromatography on p-aminomethylbenzene-sulphonamide immobilized on cyanogen-bromide-activated agarose gel (30,31). The gel column (1.6×20 cm), fitted to an AKTA FPLC system (Pharmacia, Peapack, NJ), was equilibrated with 25 mM Tris and 100 mM Na_2SO_4 adjusted to pH 8.7 with HCl, and rinsed with 25 mM Tris and 300 mM $NaClO_4$ adjusted to pH 8.7 with HCl; the enzyme was then eluted at 8 ml h^{-1} by 100 mM CH_3COOH and 500 mM $NaClO_4$, pH 5.6, at 4°C. Protein elution was monitored by measuring the eluate absorbance at 280 nm, and all fractions containing CA activity, measured by an electrometric method (30), were pooled and concentrated by ultrafiltration with YM10 membrane (Amicon, Lexington, MA) under nitrogen pressure (7×10^5 Pa). All purification steps were carried out at 4°C. Purified human erythrocyte CAII was purchased by Sigma (St. Louis, MO).

Sample preparation

Powdered solid solutions of the protein in saccharose were obtained starting from protein dialyzed against the appropriate buffer for 24 h at 4°C. Buffers were prepared for a final concentration of 100 mM using secondary and tertiary ammonium bases, such as piperazine and triethanolamine, with glycine and aliphatic carboxylic acids (32). The protein solution, at a concentration of ~10 mg/ml and containing saccharose in a saccharose/protein ratio of 3:1 w/w (corresponding to a concentration of ~0.250 g of protein per gram of final solid solution), was then rapidly frozen in liquid nitrogen and lyophilized. The solid samples of the CA form were obtained simply by lyophylization of the protein solution in the presence of the cryoprotectants.

The specimens for x-ray absorption spectroscopy measurements were prepared by pressing ~50 mg of lyophilized powdered protein solid solution under 140 atm in a small home-made press with a chamber having lateral dimensions of 2.2×0.3 cm; the slides obtained were ~0.2 cm thick.

Solutions of irradiated proteins, used to evaluate the integrity of the samples, were obtained by dissolving the corresponding slide in milliQ water and dialyzing against the appropriate buffer for 48 h at 4°C.

The XANES (X-ray Absorption Near Edge Structure) measurements were performed at the LURE synchrotron facility (Paris, France), in the D21 (EXAFS II) beamline. The Zn K-edge XANES signals were collected in fluorescence mode, at room temperature, by a seven-element Ge detector (Canberra, Meriden, CT). A Si (311) crystal was used as a monochromator. The energy range was from 9600 to 9800 eV. (Calibration of energy was performed by means of a zinc foil reference). The energy resolution was 0.3 eV, with a counting time of 6 s/point. The absorption spectra were collected using a Lambda 16 double beam spectrophotometer equipped with a thermostated cell holder (PerkinElmer, Wellesley, MA).

The XANES data analysis was performed using the Minuit XANES (MXAN) method (33), which made it possible to fit the energy region from the edge up to 200 eV above the threshold in terms of selected structural parameters.

The MXAN method performs the minimization of the residual function, R_{sq}, defined as

$$R_{sq} = \sum_{i=1}^{m} \frac{[(y_i^{th} - y_i^{exp})\varepsilon_i^{-1}]^2}{m},$$

where m is the number of experimental data, and y_i^{th} and y_i^{exp} are the theoretically computed and experimentally measured values of the absorption coefficient, respectively. Our estimate of the experimental error is ε_i, considered constant in the fitting procedure and, in our case, equal to ~0.8% of the experimental edge jump. Details of the MXAN procedure are described in (34–37).

The cluster of atoms used in the fitting procedure includes atoms up to 6.3 Å from the absorber, and the muffin-tin radii are chosen according to the Norman criterion, with a 5% overlap. The number of atoms in the cluster used for the calculation was chosen on the basis of a convergence criterion. This cluster was generated starting from the PDB coordinates of the human CAII (PDB reference, 2cba). No core hole was considered in the final-state potential.

Fitting strategy

The atomic positions are described using a polar coordinate system; the absorbing atom is placed at the origin of the coordinate frame. The atoms of one protein ligand or amino acid residue are considered as a perfectly rigid molecular group, and when the Zn-N distance is changed in the fitting, all atoms of the histidine rings move accordingly. In the fit, the bond of the Zn-O of the coordinated water molecule was allowed to vary in both length and polar angles.

The ionization energy E_o is 9660 eV (see Figs. 3 and 4), and the spectra were consistently normalized to 1. The contribution of the pre-edge energy region was subtracted using the standard procedure.

Modeling

The first step in choosing the appropriate templates was to use the structure prediction server BioInfoBank Meta Server (http://bioinfo.pl/meta/). The search can be customized choosing the prediction methods that have to be considered by 3D jury; specifically, the threading method was ''deselect''. Then, the option ''model-to-all'' was chosen, which considers the 10 best models from each server previously selected to be taken into account (38). For the modeling procedure, the Swiss Model method was used (http://swissmodel.expasy.org//SWISS-MODEL.html) in combination with the DeepView 3.7 (sp5) program (http://swissmodel.expasy.org/spdbv/).

Electrostatic potential distributions were calculated using numerical solution of the nonlinear Poisson-Boltzmann equation implemented in APBS software (http://apbs.sourceforge.net/).

All of the CA structures were superimposed and similarly oriented before the calculations. AMBER forcefield was used for partial atomic charges and radii, with internal and external dielectric constant values of 2 and 78, and solvent and ionic probe radii of 1.4 and 1.9 Å (with monovalent salt concentration of 150 mM) .

For visualization, PyMol (http://pymol.sourceforge.net/) with APBS plugin (APBS_tools.py) was used. APBS calculated values were plotted on a Gaussian-type surface, as seen below (see Fig. 2, with the color code described in the accompanying legend).

For electrostatic potential calculation, we used Hex 4.5 (http://www.csd.abdn.ac.uk/hex), which solves the differential Poisson equation for electrostatic potential and gives as output a value for the potential (in mV) for the tested protein.

To test the models, the SAVS validation server was used (http://nihserver.mbi.ucla.edu/SAVS/).

Sequence analysis

For sequence analysis, Blast (http://www.ncbi.nih.gov/BLAST/), ClustalW (http://www.ebi.ac.uk/clustalw/) and custom designed software were used.

RESULTS

Template structure for the MXAN analysis

The choice of an adequate structural template to be used in the MXAN analysis of the absorption K-edge data for Ice-CA was carried out using the Metap server. The ranking algorithm used was 3D-jury (see Materials and Methods section). The resulting structural file was made up of best-confidence predictions (all hits had a score of >226): 1flj, PDB code for S-glutathiolated *Rattus norvegicus* CAIII (rCAIII), with a resolution of 1.9 Å (39); 1v9i, *Bos taurus* CAII (BCAII), with a $Gln^{253} \rightarrow Cys^{253}$ mutation and a resolution of 2.5 Å; 2cba, *Homo sapiens* CAII (hCAII), with a high resolution of 1.54 Å (17); 12ca, hCAII with an $Ala^{121} \rightarrow Val^{121}$ mutation and a resolution of 2.40 Å (10); 1hcb, hCAI complexed with bicarbonate, with a resolution of 1.60 Å (40).

Further criteria used in the selection of the template crystallographic structure were the absence of an exogenous ligand in the active site, the presence of a wild-type sequence, and the level of resolution of the crystal structure. The application of these criteria resulted in two plausible templates: 1flj and 2cba.

To choose between these two templates, a sequence analysis was carried out among Ice-CA (SWISS-PROT Protein Data Bank under the accession number P83299), hCAII (which corresponds to the structure 2cba.pdb), and rCAIII (which corresponds to the structure 1flj.pdb) (Fig. 1). In addition to the general sequence homology, attention was given to the conserved residues believed to be involved in the reaction mechanism, the residues which in the crystal structures are close to the reaction center, and to the fully conserved residues throughout the sequence.

Using the crystal structures 2cba and 1flj and the sequence alignments of these with Ice-CA, it was possible to identify the amino acids in Ice-CA that are likely to be within 10 Å of the zinc atom. The result of the comparison of the selected amino acids indicates that Ice-CA has a higher identity with hCAII (2cba, 88%) than with rCAIII (1flj, 76%).

```
Ice-CA   .AHAWGYGPTDGPDKWVSNFPIADGPRQSPIDILPGGASYDSGLKPLSLKYDPS
hCAII    MSHHWGYGKHNGPEHWHKDFPIAKGERQSPVDIDTHTAKYDPSLKPLSVSYDQA
rCAIII   .AKEWGYASHNGPEHWHELYPIAKGDNQSPIELHTKDIRHDPSLQPWSVSYDPG

Ice-CA   NCLEILNNGHSFQVTFADDSDSSTLKEGPISGVYRLKQFHFHWGASNDKGSEHT
hCAII    TSLRILNNGHAFNVEFDDSQDKAVLKGGPLDGTYRLIQFHFHWGSLDGQGSEHT
rCAIII   SAKTILNNGKTCRVVFDDTFDRSMLRGGPLSGPYRLRQFHLHWGSSDDHGSEHT
                  *                                 *
Ice-CA   VAGTKYPAELHLVHWNTKYPSFGEAASKPDGLAVVGVFLKIGDANASLQKVLDA
hCAII    VDKKKYAAELHLVHWNTKYGDFGKAVQQPDGLAVLGIFLKVGSAKPGLQKVVDV
rCAIII   VDGVKYAAELHLVHWNPKYNTFGEALKQPDGIAVVGIFLKIGREKGEFQILLDA

Ice-CA   FNDIRAKGKQTSFADFDPSTLLPGCLDYWTYDGSLTTPPLLESVTWIVCKEPIS
hCAII    LDSIKTKGKSADFTNFDPRGLLPESLDYWTYPGSLTTPPLLECVTWIVLKEPIS
rCAIII   LDKIKTKGKEAPFNHFDPSCLFPACRDYWTYHGSFTTPPCEECIVWLLLKEPMT
                                          *
Ice-CA   VSCEQMAKFRSLLFSAEGEPECCMVDNYRPPQPLKGRHVRASFQ
hCAII    VSSEQVLKFRKLNFNGEGEPEELMVDNWRPAQPLKNRQIKASFK
rCAIII   VSSDQMAKLRSLFASAENEPPVPLVGNWRPPQPIKGRVVRASFK
```

FIGURE 1 Alignment of *C. hamatus* CA, *H. sapiens* CAII, and *R. norvegicus* CAIII. Asterisks refer to positions near the reaction center that are (typically) different in mammalian CAII and CAIII. The amino acids located (with one or more of their atoms) within 10 Å of the zinc atom are underlined.

A key residue is His^{64}, which is the proton shuttle of the reaction mechanism in all mammalian CAIIs. The His^{64} is absent in the corresponding position of rCAIII. Ice-CA has a His residue in the position corresponding to 64 in CAII. Furthermore, this His residue in Ice-CA is part of a pattern of four highly conserved residues (-GHSF-) present in mammalian CAII.

As mentioned in the Introduction, another relevant amino acid for the reactivity of CA is in position 198. This is a phenylalanine in all CAIIIs, but in both mammalian CAII and Ice-CA, it is a leucine, which provides further support for the proposed similarity between CAII and Ice-CA.

For the MXAN analysis, the cluster used to generate the simulated absorption spectra includes all atoms within 6.3 Å of the absorption center. Thus, a detailed comparison of all amino acid positions in this region in 2cba and 1flj was undertaken. An important difference is that a Phe is present in position 95 in 1flj, whereas a Leu is present in 2cba. This Leu, which is conserved in CAII, is also present in Ice-CA. All atoms of residue 95, which is present in the sequence between the two Zn-coordinating histidine residues (94 and 96), were included in the cluster used for the MXAN analysis, making 2cba the stronger candidate for template. Furthermore, among all of the structures selected by the 3D jury, 2cba had the highest resolution, confirming it as an ideal starting point for the structural simulations.

Ice-CA modeling

Starting from the Ice-CA sequence and using the 2cba structure as template (overall 62% of amino acid identity), the Swiss Model server was used to generate a molecular model of the icefish protein. The refinement of the obtained model was carried out with DeepView 3.7. The resulting model was tested using the SAVS validation server. The obtained model for Ice-CA was a starting point for other computations aimed at comparing a few relevant physical and chemical properties of Ice-CA and 2cba.

The first property analyzed was the electrostatic potential distribution using, with undistinguishable results, both Hex4.5 and APBS. The two proteins have a significantly different electrostatic potential distribution. Ice-CA has a calculated overall negative potential of −0.22 mV (using Hex4.5). The corresponding value for 2cba (with no water except the Zn-coordinated one) is +0.70 mV.

A visualization of the electrostatic potential plotted on the Gaussian-type surface is shown in Fig. 2 (generated using APBS). The difference in electrostatic potential distribution

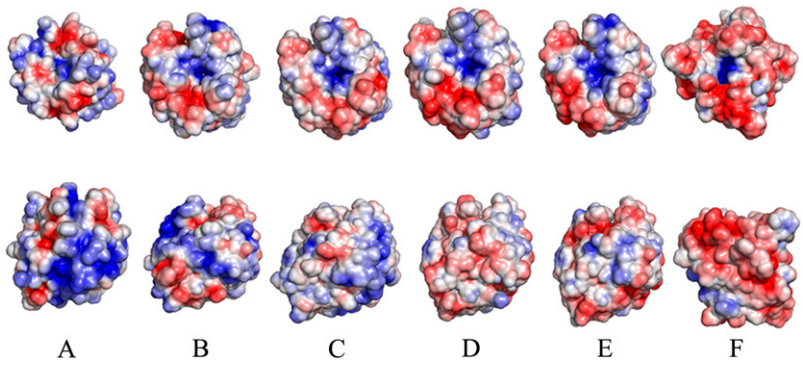

FIGURE 2 Electrostatic potential distribution mapped on the Gaussian-type surface calculated by APBS and visualized with PyMol for ZCA (*A*), hCAII (*B*), TCAb (*C*), TCAc (*D*), Ice-CA (*E*), and dCAII (*F*). The structures are graphically depicted looking down the active-site cleft (*upper row*) and in a 180°-rotated view (*lower row*). The potentials range from −1.5 kT per proton charge (*red*) to +1.5 kT per proton charge (*blue*).

between the two proteins can be attributed to both a different propensity of the intermolecular interactions and to the properties of the reaction channel that leads the substrate to the zinc atom.

To evaluate the possibility that the observed difference in electrostatic potential distribution between the generated models of Ice-CA and 2cba is more than coincidental, a broader set of high-activity carbonic anhydrase (CAII-like) was considered. These were all from fish living in temperate climates: red blood cell (rbc) CA from *Oncorhynchus mykiss* (TCAb, NCBI accession number AAP73748 (41)), rbc CAs from *Danio rerio* (ZCA, AAH57412; CAH-Z, AAH65611), cytoplasmic CA from *O. mykiss* (TCAc, AAR99329 (41)).

For all of the CAs mentioned above, a molecular model was generated (according to the procedure described for icefish CA); the sequence homologies to 2cba were 63% with ZCA, 61% with TCAb, and 63% with TCAc. For each of the resulting molecular models, the electrostatic potential distribution was calculated. The calculated potential distributions for rbc CAs are similar to that calculated for human CAII, with an overall positive potential (Fig. 2) in an uneven distribution of neutral, negative, and positive potentials throughout the molecular surface. The unusual electrostatic potential distribution observed for Ice-CA was also found in the molecular model generated for TCAc. This cytosolic isoform is also found in gills and has a catalytic activity lower than that of the rbc *O. mykiss* CA isoform (41). For comparative purposes, the electrostatic potential distribution was also calculated for the CA of the salt-tolerant unicellular green alga *Dunaliella salina* (PDB code 1y7w (42)).

XANES/MXAN analysis on Ice-CA and hCAII

In Fig. 3, the normalized experimental K-edge absorption spectra are presented for both the human and the icefish CA. The two spectra do not show any chemical shift in the time course of the measurements. The most important difference between the two spectra is the feature at ~10 eV, which is sharper in the icefish protein (Fig. 3, *curve A*). The best fit of the K-edge absorption spectra of the hCAII is presented in Fig. 4 *A*. The agreement between the experimental data and the calculated spectra is excellent over all spectral regions. The R_{sq} value of the best fit is 4.06. The starting atomic coordinates for the fitting procedure were those obtained from the 2cba PDB file, obtained from the crystal structure of CAII from human erythrocytes. The one-shot calculation of the edge spectra using the crystallographic coordinates gives an R_{sq} value of 13.77. The bond length values obtained from the fitting procedure for both proteins are reported in Table 1, along with those obtained from the crystal structure of 2cba for comparison. The human protein has a greater asymmetric distribution of Zn-N distances, which results in a statistically significant difference. Furthermore, the B factors for both the Zn and the atoms of the metal ligands in the 2cba PDB file lead to an expected uncertainty for the bond lengths in the crystallographic data of ~0.25 Å. The reported Zn-O distance for the water molecule coordinated to the Zn atom

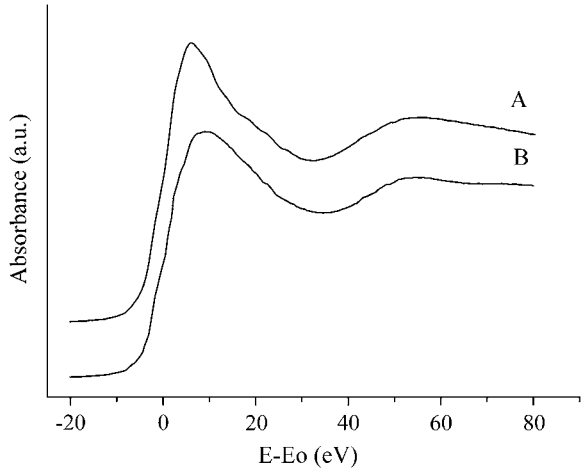

FIGURE 3 Zn K-edge XANES experimental spectra for Ice-CA *C. hamatus* (*A*) and hCAII *H. sapiens* (*B*).

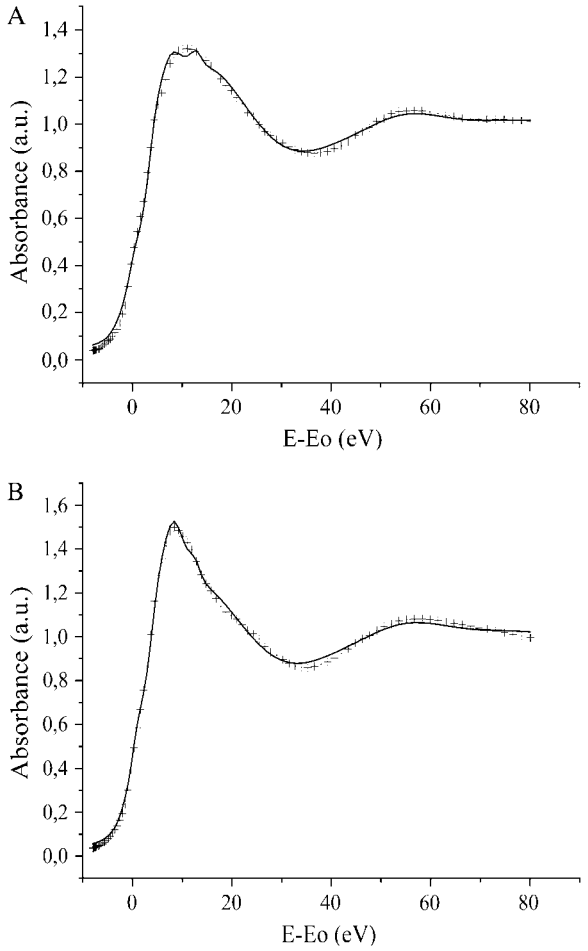

FIGURE 4 Comparison of the best-fit calculation (*solid line*) and the experimental data (*crosses*) of hCAII (*A*) and Ice-CA (*B*).

TABLE 1 Bond lengths obtained for the best-fit procedures for the experimental data

	Ice-CA	hCAII	2cba
d(Nε His^{94}-Zn)	2.044 (± 0.0001)*	1.996 (± 0.035)	2.10 (± 0.25)†
d(Nε His^{96}-Zn)	2.076 (± 0.033)	2.137 (± 0.034)	2.12 (± 0.25)†
d(Nδ His^{119}-Zn)	2.084 (± 0.046)	2.045 (± 0.036)	2.11 (± 0.25)†
d(HOH^{263}-Zn)	2.044 (± 0.0001)*	1.996 (± 0.020)	2.05 (± 0.32)†
d(OγThr^{199}-Zn)	4.060 (± 0.059)	3.913 (± 0.038)	3.93 (± 0.25)†

The crystallographic bond lengths extracted from the crystal structure of human carbonic anhydrase II (*2cba*) are presented for comparison.
*In considering the reported error value of the statistical error (evaluated by the MIGRAD subroutine of the MINUIT program (F. James, CERN, Geneva), it should be mentioned that the systematic error is on the order of 1%, as inferred for previous work on model systems.
†The reported uncertainty in distances represents the root mean-square deviation calculated from the individual B values reported in the PDB file.

(H_2O 263 in 2cba) shows an even higher value for the B factors, which further increases the uncertainty to 0.32 Å. Fig. 4 *B* shows the best fit of the K-edge absorption spectra of cytosolic CA from *C. hamatus*. The agreement between the experimental data and the calculated spectra is again excellent over all spectral regions, and the R_{sq} value of the best fit is 4.44. The rationale for the choice of starting coordinates for the MXAN analysis has been presented above in part. Further considerations relate to the result of the simulations of the edge spectrum based only on the coordinates of the crystal-structure 2cba ($R_{sq} = 27.36$) and 1flj ($R_{sq} = 38.79$), which indicate a higher structural similarity of the considered atom cluster for the human enzyme. As mentioned above, a further advantage of the 2cba PDB file is its higher resolution. On these bases, 2cba was used as the template structure for the MXAN fitting procedure for both proteins.

Among the structural parameters explored in the fitting procedure, the most important are the H_2O263-zinc distance (Fig. 5 *A*) and the θ angle (Fig. 5 *B*) for the Zn-coordinated water molecule. The H_2O263-zinc distance turned out to be the more relevant structural feature, as can be seen in Fig. 5 *A*. The θ angle for the Zn-coordinated water molecule shows a less pronounced minimum in the R_{sq} profile for both proteins. (For clarity, only the data for the human protein is reported in Fig. 5 *B*).

The other determinant structural parameters were the θ angle and the distance from the Zn atom and Oδ of Thr^{199}. In comparing hCAII and Ice-CA, some important considerations are due on the interplay of zinc-coordinated water and Thr^{199}. In the structural models of the active site obtained in the fitting procedure, a different position is observed for Thr^{199} (Fig. 6). The Zn-Oδ (Thr^{199}) distance is shorter in hCAII as is the Zn-O (H_2O263) distance. This is consistent with the observation that Thr^{199} and the coordinated H_2O are involved in the H-bond network that represents one of the most conserved structural features of cytosolic carbonic anhydrases (CAI, CAII, and CAIII).

The zinc-coordinated histidines, which in the fitting procedure were allowed to move, were not effective parameters

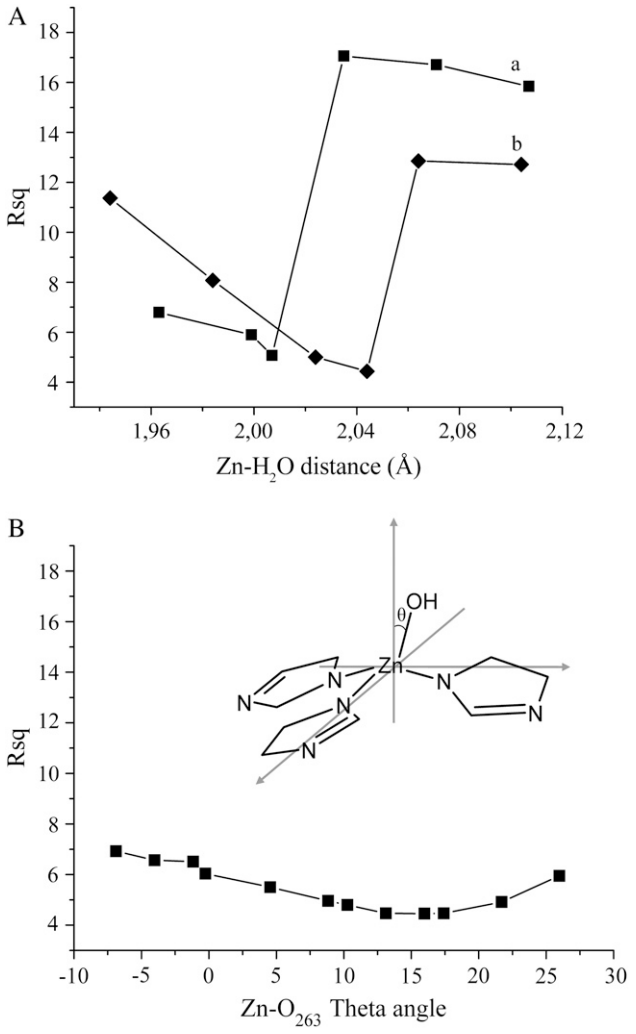

FIGURE 5 (*A*) R_{sq} profile as a function of the bond length of Zn-O of the H_2O 263 for hCAII (*a*) and Ice-CA (*b*). (*B*) R_{sq} profile as a function of the θ angle between the *z* axis and the Zn-O bond. For simplicity, the 0° value corresponds to the orientation of the Zn-O bond in the crystal structure of 2cba.

in the optimization of the fit. The final structural model and the relative bond lengths are presented in Fig. 6 and Table 1, respectively. The histidines' ligands are almost superimposable and are not likely to be responsible for the difference between the two proteins analyzed. The first observation is on the comparison between the structural data obtained from the fitting of the human protein and the available crystallographic structure 2cba. As shown in Table 1, the differences for all considered parameters are within the values of the associated errors. These must be compared to the crystallographic data, which are less precise. In comparing the structural models obtained for the human protein and Ice-CA, a general shortening of bond distances is observed in the reaction center that averages −0.05 Å.

Taking into account the high resolution of the MXAN analysis, we observe that Zn-nitrogen distances are not equivalent

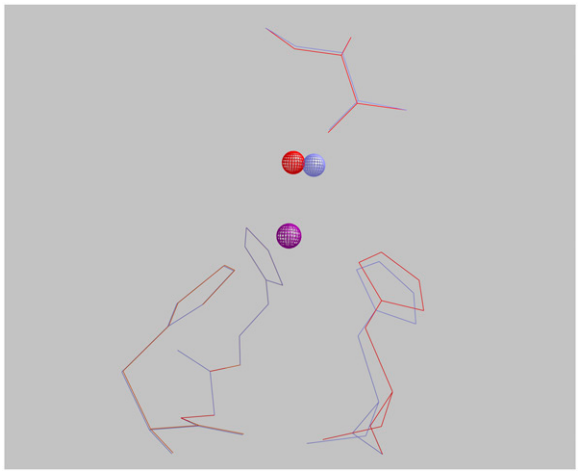

FIGURE 6 Comparison between the structural models of the reaction centers of Ice-CA (*blue*) and hCAII (*red*) obtained in the MXAN analysis. Zinc atom (*violet*) and coordinated waters are shown in ball-and-stick mode, whereas Thr^{199} and coordinated histidines are shown in a wire-frame mode. In addition to the three coodinating histidine residues on the left side of the figure, Thr^{199} is also shown.

for the coordinated histidine. This observation, at least for the human protein, seems to be in contrast with the crystallographic data. However, as previously observed, the magnitude of the differences in distance that generate this asymmetry is smaller than the error associated with the crystallographic data but larger than the estimated error in the MXAN analysis.

The Zn-O distance for the coordinated water molecule is 0.048 Å, a value that seems to be very significant for the low errors associated with the MXAN distance determination. To further enforce this observation, a series of simulations was made to single out the effect of both the Zn-O distance and the θ angle on the R_{sq} value. Starting from the best-fit structure for the two proteins, we generated individual simulations in which only the Zn-O distance was changed stepwise. Fig. 5 *A* plots the R_{sq} value against the Zn-O distance. The individual curves for the two proteins show a well-defined difference in the minima for the explored parameter, providing strong support for the claimed difference in distance for the coordinated water molecule in the two proteins. These two minima are not superimposable, demonstrating that this difference can be considered highly significant from a statistical point of view. As will be discussed later, the implications of this difference are of importance for the functional properties of CA. A similar analysis was conducted on both proteins for the coordinated water and θ-angle parameter. The dependence of fit on this parameter is present only in the human protein. The results of this analysis are shown in Fig. 5 *B*. A shallow minimum is observed at ~15° (assuming the position derived from 2cba as 0°). However, this parameter has a lower impact on the fit when compared with the Zn-O distance. Superimposition of the best-fit corresponding structures for Ice-CA and hCAII is shown in Fig. 6.

DISCUSSION

To define the molecular basis of cold adaptation, it is important to characterize the structure of those proteins that, for their physiological roles, are more likely to be modified in the process. Carbonic anhydrase is one of these potential target enzymes for its key role in a number of cellular functions. In this study, as a paradigm of cold-adaptation molecular mechanisms, the structural characteristics of a soluble CA isoform isolated from the gills of an Antarctic hemoglobinless fish, *C. hamatus*, were compared to those of other mesophilic CAs.

Among the CA sequences of teleosts, an average identity of 75% was found. Specifically, the CA from *C. hamatus* was compared with the different isoforms known of *D. rerio* and *O. mykiss*. Identity ranges from 70% with ZCA and 77% with CAH-Z of *D. rerio* to 79% with gill CA (TCAc, also signed as a CAI-like isoform, *O. mykiss* CAI) and 77% of rbc CA (TCAb, also signed as a CAII-like isoform *O. mykiss* CAII) from *O. mykiss*.

Comparison of the Ice-CA sequence with α CAs present in the PDB structural database indicates a larger similarity with mammalian CAII than other mammalian isoforms for the amino acids within 10 Å (Fig. 1) of the catalytic zinc atom, which are more likely to play a key role in the reaction mechanism.

Some further considerations are due on the residues that define the completely conserved local chemical environment of the zinc atom. The first group of conserved amino acids is involved in proton shuttling (Gly^{65}, His^{64}, Ser^{65}/Ala^{65}, and Phe^{66}, using a numbering that is valid for all mammal CAIIs), where serine is always present in position 65 except in the human enzyme, where an alanine is present. The presence of a relatively small amino acid (i.e., Ala or Ser) in proximity to the proton shuttle His^{64} does not affect either the mobility of the latter or, consequently, the kinetic parameters of the enzyme.

The second group of conserved amino acids defines the hydrophobic pocket (Val^{121}, Val^{143}, Trp^{209}, and Leu^{198}) that is conserved in Ice-CA and in all mammalian CAIIs.

A third class of extremely conserved amino acids in all CAs from vertebrates is that in the second coordination shell of the metal ion in the active site. These are the residues that form a hydrogen bond to the noncoordinating nitrogen of the zinc ligand histidines (Gln^{92} with His^{94}, Glu^{117} with His^{119}, and Asn^{244} with His^{96}) and to the fourth metal ligand, the exchangeable water molecule (Thr^{199}).

However, some amino acids in positions close to the zinc atom are different in icefish CA compared to human CA. These are Leu and Ile in positions 144 and 146 for hCAII, and valines in the same positions for icefish . It should be mentioned that these positions are not particularly conserved among CAs from vertebrates, although the variability is confined to Leu, Ile, and Val. For example, CAs from *B. taurus* and *Ovis aries* show the same amino acids in this region as CAs from icefish, whereas *D. rerio* CAII has Val^{144} and Ile^{146}.

The last relevant difference between hCAII and Ice-CA is in position 245, which is always a Trp in mammals and a Tyr among fish. This is a position difference between fish and mammals and not a peculiarity of icefish.

In conclusion, the comparative analysis of amino acids located within 10 Å of the zinc atom allows the identification of key residues in the reaction mechanism that represent criteria in the diversification of the various CA isoforms. However, no indication emerges for a unique sequence feature of icefish CA that can rationalize the low-temperature adaptation simply by referring to the amino acids close to the zinc. The amino acid conservation, as expected, decreases moving away from the zinc atom. Consequently, it becomes difficult to assign relevance to any of the observed differences between icefish CA and other CAs in the database.

On these premises, the most plausible structural template to be used as a starting point for the MXAN analysis is hCAII (PDB code 2cba). As mentioned above, the simulation of the K-edge absorption spectra using MXAN allows for the definition of a structural model of the active site where the position of the individual atoms of the protein is defined up to ~6 Å from the zinc atom. The experimental strategy implied the measurement of a known sample of hCAII to be used as a validation test for the analysis of the structurally unknown Ice-CA. The structural metric of the active site of hCAII coming from the MXAN analysis is in substantial agreement with the crystallographic data. The limit in this comparison is caused by the resolution of the crystal structure, which permits errors in the atomic positions larger than the observed differences. On the other hand, the accuracy of the MXAN analysis allows discrimination between the human and icefish proteins, highlighting the structural differences between the active sites.

The Zn-coordinated water molecule is an essential player in the reaction mechanism of CA; consequently, the definition of the bond length was of key importance. As observed in Fig. 5 *A*, the proposed difference between hCAII and Ice-CA is substantiated by the presence of two distinct minima when the R_{sq} value is plotted against bond length. A further difference between hCAII and Ice-CA is the angle of the Zn-H_2O bond with the plane, defined by the three coordinating nitrogen atoms of the histidine ligands. As observed in Fig. 5 *B*, the effect is less pronounced than that observed for bond length, but a minimum in R_{sq} value is still observed.

A structural feature that relates to those mentioned above is the position of the δO of Thr^{199}, an atom in the crystal structures that is always reported to be hydrogen-bonded to the Zn-coordinated water molecule. In the R_{sq} minimization procedure, the movement of this atom, placed at 3.9 Å from the zinc atom, is correlated with the movement of the Zn-coordinated water molecule, even when these two atoms are allowed to move independently. Consequentially, a shorter Zn-δOThr^{199} distance corresponds also to the shorter Zn-H_2O bond length of the hCAII. It is tempting to propose that all of these structural differences concur to the modulation of the pK value of the coordinated water molecule in the two proteins, but no reliable correlation has been defined between these structural features and the actual pK values, which are also likely to depend on other properties, such as the local dielectric constant.

No simple correlation can be made between the observed structural difference in the active site and the amino acid composition for the region around the metal center. The amino acid conservation is complete between hCAII and Ice-CA for the amino acids within a sphere of radius 6 Å centered on the zinc atom. The features that define the observed differences in structure and kinetic properties between these two proteins must be related to something other than what is usually described as governing the molecular mechanism of CA, i.e., Thr^{199}, the hydrophobic pocket, and the region around the proton shuttle.

The final step in the structural analysis presented here was the generation of a molecular model of Ice-CA by homology modeling of the template provided by the PDB file of hCAII. The electrostatic potential was calculated for both the generated model of Ice-CA and the crystallographic structure of hCAII. A striking difference emerged from the comparison: an overall negative potential for Ice-CA (−0.2 mV) and a significant positive potential for hCAII (+0.7 mV).

This difference can be easily visualized when the two proteins are presented using a color coding that refers to the surface potential (Fig. 2, *A* and *E*). The surface potential distribution is substantially different, with a difference in the region of the substrate entrance to the active site, but more pronounced in the back side of the protein.

To evaluate the observed differences in surface potential for a larger set of CAs, the molecular modeling was extended to other fish CAs: *D. rerio* CA (ZCA, sequence identity with hCAII 63%), *O. mykiss* rbc CA (TCAb, sequence identity with hCAII 61%) and *O. mykiss* cytosolic CA (TCAc, sequence identity with hCAII 63%). For all of the molecular models, the surface potentials were calculated, with the results reported in Fig. 2. The two CAs from erythrocytes show an electrostatic potential distribution similar to hCAII, with an overall positive potential. On the other hand, the cytosolic CA from *O. mykiss* shows an overall negative electrostatic potential distribution very similar to that of Ice-CA.

The latter result suggests a diversification of fish CAs based more on cell type than on species. In this regard, in a recent study on the CA of a green alga, *D. salina* (42), a relationship has been proposed between the halo tolerance of this organism and the observed electrostatic potential distribution reported in Fig. 2 *F* for comparison. The authors emphasize the relation between the overall very negative electrostatic potential and the interaction with anions (particularly halides). More precisely, the low potential in the reaction center associated with the surface potential could rationalize the modulation in the affinity constant of the zinc atom in the active site toward halide binding, together with

the other unusual properties of solubility and stability of the algae CA.

The negative electrostatic potential of the branchial Ice-CA and TCAc isoforms could be responsible for their substrate affinity values being significantly lower than those reported for trout rbc CA (30,41). Moreover, a different electrostatic potential in and around the active site of gill Ice-CA could also explain the observed high catalytic rates at low temperatures (30), with the consequent advantages of a rapid interconversion of CO_2/HCO_3^- in the blood despite the lack of a circulating CA in Antarctic hemoglobinless teleosts (30). According to the structural features already found in other cold-adapted enzymes (43,44), as, for example, subtilisins excreted by Antarctic bacteria (45), a high number of negative-charge residues at low temperatures could improve the protein-surface interactions with the solvent, the flexibility of the enzyme structure, and the positioning of the substrates in the active site.

On these bases, the predicted difference in the electrostatic potential between hCAII and Ice-CA represents the best candidate to justify the measured structural differences between these two proteins. The modulation of the interaction between the catalytic water molecule and the zinc atom could, as demonstrated for an analogous interaction of halides, depend on the effect of the electrostatic potential distribution. It should be mentioned, however, that the electrostatic potential distribution itself, being substantially comparable in only the two cytosolic fish CA considered, may be not sufficient to account for the cold adaptation of this molecule, hence calling for future studies on other cold-adapted species.

This work is in the framework of the Italian National Program for Antarctic Research. The authors thank Dr. Isabella Ascone for excellent technical support at the LURE facility and Prof. Federico Fogolari for helpful discussions on the manuscript.

REFERENCES

1. Hewett-Emmett, D., and R. E. Tashian. 1996. Functional diversity, conservation, and convergence in the evolution of the α-, β-, and γ-carbonic anhydrase gene families. *Mol. Phylogenet. Evol.* 5:50–77.
2. So, A. K., G. S. Espie, E. B. Williams, J. M. Shively, S. Heinhorst, and G. C. Cannon. 2004. A novel evolutionary lineage of carbonic anhydrase (ε class) is a component of the carboxysome shell. *J. Bacteriol.* 186:626–630.
3. Sawaya, M. R., G. C. Cannon, S. Heinhorst, S. Tanaka, E. B. Williams, T. O. Yeates, and C. A. Kerfeld. 2006. The structure of β-carbonic anhydrase from the carboxysomal shell reveals a distinct subclass with one active site for the price of two. *J. Biol. Chem.* 281:7546–7555.
4. Tashian, R. E., D. Hewett-Emmett, N. Carter, and N. C. Bergenhem. 2000. Carbonic anhydrase (CA) -related proteins (CA-RPs), and transmembrane proteins with CA or CA-RPdomains. *EXS.* 90: 105–120.
5. Hewett-Emmett, D. 2000. Evolution and distribution of the carbonic anhydrase gene families. *In* The Carbonic Anhydrases: New Horizons, W. R. Chegwidden, N. D. Carter, and Y. H. Edwards, editors. Birkhäuser Verlag, Boston. 29–76
6. Lindskog, S. 1997. Structure and mechanism of carbonic anhydrase. *Pharmacol. Ther.* 74:1–20.
7. Christianson, D. W., and C. A. Fierke. 1996. Carbonic anhydrase: evolution of the. zinc binding site by nature and by design. *Accounts Chem. Res.* 29:331–339.
8. Christianson, D. W., and J. D. Cox. 1999. Catalysis by metal-activated hydroxide in zinc and manganese metalloenzymes. *Annu. Rev. Biochem.* 68:33–57.
9. Tripp, B. C., K. Smith, and J. G. Ferry. 2001. Carbonic anhydrase: new insights for an ancient enzyme. *J. Biol. Chem.* 276:48615–48618.
10. Nair, S. K., T. L. Calderone, D. W. Christianson, and C. A. Fierke. 1991. Altering the mouth of a hydrophobic pocket. Structure and kinetics of human carbonic anhydrase II mutants at residue Val-121. *J. Biol. Chem.* 266:17320–17325.
11. Steiner, H., B. H. Jonsson, and S. Lindskog. 1975. The catalytic mechanism of carbonic anhydrase. Hydrogen-isotope effects on the kinetic parameters of the human C isoenzyme. *Eur. J. Biochem.* 59:253–259.
12. Tu, C. K., D. N. Silverman, C. Forsman, B. H. Jonsson, and S. Lindskog. 1989. Role of histidine 64 in the catalytic mechanism of human carbonic anhydrase II studied with a site-specific mutant. *Biochemistry.* 28:7913–7918.
13. Shimahara H., T. Yoshida, Y. Shibata, M. Shimizu, Y Kyogoku, F. Sakiyama, T. Nazakawa, S. Tate, S. Ohki, T. Kato, H. Moriyama, K. Kishida, Y. Tano, T. Ohkubo, and Y. Kobayashi. 2007. Tautomerism of histidine 64 associated with proton-transfer in catalysis of carbonic anhydrase. *J. Biol. Chem.* 282:9646–9656.
14. Khalifah, R. G. 1971. The carbon dioxide hydration activity of carbonic anhydrase. I. Stop-flow kinetic studies on the native human isoenzymes B and C. *J. Biol. Chem.* 246:2561–2573.
15. Engstrand, C., B. H. Jonsson, and S. Lindskog. 1995. Catalytic and inhibitor-binding properties of some active-site mutants of human carbonic anhydrase I. *Eur. J. Biochem.* 229:696–702.
16. Jewell, D. A., C. K. Tu, S. R. Paranawithana, S. M. Tanhauser, P. V. LoGrasso, P. J. Laipis, and D. N. Silverman. 1991. Enhancement of the catalytic properties of human carbonic anhydrase III by site-directed mutagenesis. *Biochemistry.* 30:1484–1490.
17. Hakansson, K., M. Carlsson, L. A. Svensson, and A. Liljas. 1992. Structure of native and apo carbonic anhydrase II and structure of some of its anion-ligand complexes. *J. Mol. Biol.* 227:1192–1204.
18. Duda, D. M., C. Tu, S. Z. Fisher, H. An, C. Yoshioka, L. Govindasamy, P. J. Laipis, M. Agbandje-McKenna, D. N. Silverman, and R. McKenna. 2005. Human carbonic anhydrase III: structural and kinetic study of catalysis and proton transfer. *Biochemistry.* 44:10046–10053.
19. Eriksson, A. E., T. A. Jones, and A. Liljas. 1988. Refined structure of human carbonic anhydrase II at 2.0 Å resolution. *Proteins.* 4:274–282.
20. Merz, K. M., Jr. 1990. Insights into the function of the zinc hydroxide-Thr^{199}-Glu^{106} hydrogen bonding network in carbonic anhydrases. *J. Mol. Biol.* 214:799–802.
21. Krebs, J. F., J. A. Ippolito, D. W. Christianson, and C. A. Fierke. 1993. Structural and functional importance of a conserved hydrogen bond network in human carbonic anhydrase II. *J. Biol. Chem.* 268:27458–27466.
22. Scolnick, L. R., and D. W. Christianson. 1996. X-ray crystallographic studies of alanine-65 variants of carbonic anhydrase II reveal the structural basis of compromised proton transfer in catalysis. *Biochemistry.* 35:16429–16434.
23. Perry, S. F., and P. Laurent. 1990. The role of carbonic anhydrase in carbon dioxide excretion, acid-base balance and ionic regulation in aquatic gill breathers. *In* Animal Nutrition and Transport Processes. 2. Transport, Respiration and Excretion, Vol. 6. J.-P. Truchot and B. Lahlou, editors. Karger, Basel. 39–57.
24. Henry, R. P., and E. R. Swenson. 2000. The distribution and physiological significance of carbonic anhydrase in vertebrate gas exchange organs. *Respir. Physiol.* 121:1–12.
25. Heisler, N. 1984. Acid-base regulation in fishes. *In* Fish Physiology, Vol X. W. S. Hoar and D. J. Randall, editors. Academic Press, New York. 315–401.

26. MacDonald, J. A., and R. M. G. Wells. 1991. Viscosity of body fluids from Antarctic Notothenioid fish. *In* The Biology of Antarctic Fishes. Springer Verlag, Berlin. 145–162.

27. Feller, G., and C. Gerday. 1997. Psychrophilic enzymes: molecular basis of cold adaptation. *Cell. Mol. Life Sci.* 53:830–841.

28. Rahim, S. M., J. P. Delaunoy, and P. Laurent. 1988. Identification and immunocytochemical localization of two different carbonic anhydrase isoenzymes in teleostan fish erythrocytes and gill epithelia. *Histochemistry.* 89:451–459.

29. Henry, R. P., and T. A. Heming. 1998. Carbonic anhydrase and respiratory gas exchange. *In* Fish Physiology Haemoglobin and Respiration, Vol. 17. S. F. Perry and B. L. Tufts, editors. Academic Press, San Diego. 75–111.

30. Maffia, M., A. Rizzello, R. Acierno, M. Rollo, R. Chiloiro, and C. Storelli. 2001. Carbonic anhydrase activity in tissues of the icefish *Chionodraco hamatus* and of the red-blooded teleosts *Trematomus bernacchii* and *Anguilla anguilla*. *J. Exp. Biol.* 204:3983–3992.

31. Whitney, P. L. 1974. Affinity chromatography of carbonic anhydrase. *Anal. Biochem.* 57:467–476.

32. Ascone, I., A. Sabatucci, L. Bubacco, P. Di Muro, and B. Salvato. 2000. Saccharose solid matrix embedded proteins: a new method for sample preparation for x-ray absorption spectroscopy. *Eur. Biophys. J.* 29:391–397.

33. Benfatto, M., and S. Della Longa. 2001. Geometrical fitting of experimental XANES spectra by a full multiple-scattering procedure. *J. Synchrotron Radiat.* 8:1087–1094.

34. Della Longa, S., A. Arcovito, M. Girasole, J. L. Hazemann, and M. Benfatto. 2001. Quantitative analysis of x-ray absorption near edge structure data by a full multiple scattering procedure: the Fe-CO geometry in photolyzed carbonmonoxy-myoglobin single crystal. *Phys. Rev. Lett.* 87:155501.

35. Benfatto, M., S. Della Longa, and C. R. Natoli. 2003. The MXAN procedure: a new method for analysing the XANES spectra of metallononeproteins to obtain structural quantitative information. *J. Synchrotron Radiat.* 10:51–57.

36. Frank, P., M. Benfatto, R. K. Szilagyi, P. D'Angelo, S. Della Longa, and K. O. Hodgson. 2005. The solution structure of $[Cu(aq)]^{2+}$ and its implications for rack-induced bonding in blue copper protein active sites. *Inorg. Chem.* 44:1922–1933.

37. Sarangi, R., M. Benfatto, K. Hayakawa, L. Bubacco, E. I. Solomon, K. O. Hodgson, and B. Hedman. 2005. MXAN analysis of the XANES energy region of a mononuclear copper complex: applications to bioinorganic systems. *Inorg. Chem.* 44:9652–9659.

38. Ginalski, K., A. Elofsson, D. Fischer, and L. Rychlewski. 2003. 3D-jury: a simple approach to improve protein structure predictions. *Bioinformatics.* 19:1015–1018.

39. Mallis, R. J., B. W. Poland, T. K. Chatterjee, R. A. Fisher, S. Darmawan, R. B. Honzatko, and J. A. Thomas. 2000. Crystal structure of S-glutathiolated carbonic anhydrase III. *FEBS Lett.* 482:237–241.

40. Kumar, V., and K. K. Kannan. 1994. Enzyme-substrate interactions. Structure of human carbonic anhydrase I complexed with bicarbonate. *J. Mol. Biol.* 241:226–232.

41. Esbaugh, A. J., S. F. Perry, M. Bayaa, T. Georgalis, J. Nickerson, B. L. Tufts, and K. M. Gilmour. 2005. Cytoplasmic carbonic anhydrase isozymes in rainbow trout *Oncorhynchus mykiss*: comparative physiology and molecular evolution. *J. Exp. Biol.* 208:1951–1961.

42. Premkumar, L., H. M. Greenblatt, U. K. Bageshwar, T. Savchenko, I. Gokhman, J. L. Sussman, and A. Zamir. 2005. Three-dimensional structure of a halotolerant algal carbonic anhydrase predicts halotolerance of a mammalian homolog. *Proc. Natl. Acad. Sci. USA.* 102:7493–7498.

43. Davail, S., G. Feller, E. Narinx, and C. Gerday. 1994. Cold adaptation of proteins. Purification, characterization, and sequence of the heat-labile subtilisin from the antarctic psychrophile Bacillus TA41. *J. Biol. Chem.* 269:17448–17453.

44. Feller, G., F. Payan, F. Theys, M. Qian, R. Haser, and C. Gerday. 1994. Stability and structural analysis of α-amylase from the antarctic psychrophile *Alteromonas haloplanctis* A23. *Eur. J. Biochem.* 222:441–447.

45. Narinx, E., E. Baise, and C. Gerday. 1997. Subtilisin from psychrophilic Antarctic bacteria: characterization and site-directed mutagenesis of residues possibly involved in the adaptation to cold. *Protein Eng.* 10:1271–1279.